Nanomanufacturing and Metrology (2023) 6:18
https://doi.org/10.1007/s41871-023-00190-w

ORIGINAL ARTICLE

Laser Ablation and Chemical Oxidation Synergistically Induced Micro/Nano Re-entrant Structures for Super-Oleophobic Surface with Cassie State

Jiaqi Chao[1,2] · Faze Chen[1,2] · Lei Xia[1,2] · Zexin Cai[1,2] · Fujun Wang[1,2] · Yanling Tian[3] · Dawei Zhang[1,2]

Received: 17 December 2022 / Revised: 7 March 2023 / Accepted: 8 March 2023

Abstract

Generally, re-entrant structures are a key part of fabricating superoleophobic surfaces, and this structure appears in almost all kinds of published research articles regarding superoleophobicity. However, the application of related fabrication methods is usually too complex and costly in real practice. In this paper, we present a simple method to generate micro-cauliflower structures, which work as re-entrant structures in microcone arrays, to promote the formation of superoleophobic surfaces. The heating process after alkali-assisted surface oxidation is the main reason for the appearance of a micro-ball structure, and the oxidation time can influence the size of the micro-ball. To the best of our knowledge, the influence of the heating process after alkali-assisted surface oxidation on the birth of the micro-ball structure is seldom researched. A low-surface-energy treatment was also analyzed in influencing the size of the re-entrant structure and its relative wettability. Droplets of 5 µl of *n*-decane show contact angles of $155 \pm 1°$on the as-prepared superoleophobic surface, and air pockets can be clearly seen underneath, indicating a stable Cassie contacting state and a promising application value in the near future.

Highlights

1. A hybrid method with concise process of fabricating superoleophobic surfaces was shown.
2. The influence of heating process after alkali-assisted surface oxidation was investigated.
3. Superoleophobic surface with clear Cassie state was fabricated.

Keywords Superoleophobic · Re-entrant structure · Cassie state · Laser direct writing

1 Introduction

During the past several decades, extreme nonwetting surfaces have been the research hotpot among researchers [1–4]. These nonwetting surfaces can also be applied in different areas, such as oil transportation, oil–water separation, micro-droplet manipulation [5], self-cleaning [6], and anticorrosion. Generally, a surface with a static water contact angle greater than 150° and a dynamic water roll-off angle below 10° is defined as a superhydrophobic surface [7–9]. A similar definition can also be used in superoleophobic surfaces [10, 11]. The so-called "oil" refers to liquids with relatively low surface tension (lower than water; $\gamma < 72.1$ mN m^{-1}), so a superoleophobic surface usually includes a

✉ Faze Chen
faze.chen@tju.edu.cn

1 School of Mechanical Engineering, Tianjin University, Tianjin 300072, China

2 Key Laboratory of Mechanism Theory and Equipment Design of Ministry of Education, Tianjin University, Tianjin 300072, China

3 School of Engineering, University of Warwick, Coventry CV4 7DL, UK

Published online: 25 May 2023

superhydrophobic surface, except for some special surfaces with peculiar chemical components [12–14]. Superoleophobic surfaces have a broader application prospect than superhydrophobic surfaces, and the former are, without a doubt, harder than the latter [15, 16]. In 1997, the first article on superoleophobic surface fabrication was written and published by Tsujii et al. [17, 18]. In their opinion, only a solid surface tension lower than a quarter of the liquid surface tension ($\gamma_S < \gamma_L/4$) can make a smooth surface oleophobic (CA > 90°). They finally obtained a superoleophobic surface with a rapeseed oil droplet contact angle of 150° via anodization and chemical medication on an aluminum plate, followed by immersing the plate in an ethanolic solution of fluorinated monoalkyl phosphates. In 2001, Li et al. prepared aligned carbon nanotube films with a fluoroalkylsilane coating, which showed superamphiphobic (both superhydrophobic and superoleophobic) properties with water and rapeseed oil contact angles of $171 \pm 0.5°$ and $161 \pm 1.0°$, respectively [19]. In 2004, Xie et al. used a one-step process to successfully fabricate superamphiphobic films [20]. Two polymer materials, i.e., polymethylmethacrylate and fluorine-end-capped polyurethane, were used in this process, and the whole process did not need any further surface modification.

Before 2007, very few articles about superoleophobicity were published due to the limitation of the superoleophobic theory. In the last 15 years, there has been rapid development in the research of superoleophobic surfaces [21, 22]. In 2007, Tuteja et al. first introduced the re-entrant surface curvature as the third parameter (besides surface roughness and chemical component) to design superoleophobic surfaces [23]. The so-called "re-entrant structure" generally includes a T-shaped structure, a mushroom-like structure, an overhang structure, an inverted trapezoid structure, a matchstick-like structure, and some other irregular microstructures [11]. The new concept of the re-entrant structure has greatly energized the oil-repellent field, and the related development has stepped into a new stage. The existence of re-entrant structures is so crucial in superoleophobicity because they can provide an upward pressure to balance the downward Laplace pressure and droplet gravity [24]. In 2014, a normal re-entrant structure was upgraded to a double re-entrant structure by Liu et al. [25]. They found that microscale posts with double nanoscale vertical overhangs can repel almost all available liquids, even perfluorohexane, whose surface tension could go as low as under 10 mN m^{-1}.

Although the key point of oil-repellent surface fabrication is to generate a re-entrant structure, the method varies, including chemical etching, solution–immersion, template, and photoetching, but most of them are not suitable for real practice [26, 27]. In 2019, Li et al. designed transparent superamphiphobic surfaces with a matchstick-like structure [28]. Micropillar arrays were obtained from a negative photoresist via standard photolithography, and a micro re-entrant poly(dimethylsiloxane) (PDMS) ball was designed using a spin-coating method and transferred technique. Moreover, the nano re-entrant structure was served by fluorinated candle soot, then they were transferred onto the micro PDMS ball, and the micro/nano re-entrant-coordinated superamphiphobic surface was finally obtained. In spite of exquisite micro/nanostructure arrays and excellent oil-repellent ability, the fabricating method was too technically cumbersome and time-consuming, so this technology needs a long way to serve factories and the public. In 2013, Ou et al. reported a convenient way to fabricate superoleophobic surfaces via strong acid etching and alkali-assisted surface oxidation, followed by surface fluorination [29]. The solution–immersion approach seems to be convenient and efficient. However, the utilization of strong acid (concentrated nitric acid in this paper) can cause environmental pollution, and toxic gases may be generated during the process. As the advantages of laser processing have been discovered, more researchers have chosen the laser direct writing technique to process micro/nanostructures [30–32].

Laser–chemical hybrid method is an economical and efficient way to produce micro/nanostructures, including re-entrant structures [33–35]. In 2018, Han et al. obtained durable superamphiphobic surfaces via a laser–chemical hybrid method consisting of ultrafast laser ablation and chemical oxidation, followed by a fluorination treatment [36]. As they reported, the prepared superamphiphobic surface could show a static dodecane droplet contact angle of > 150°, but liquids with low surface tension, such as *n*-decane droplets, were not mentioned in this paper. Furthermore, the imported ultrafast laser machine greatly increased the production cost, which is not preferable for large-scale applications [35]. In this paper, we propose a similar laser–chemical hybrid method to fabricate superoleophobic surfaces. Different from previous studies, we used a nanosecond laser machine to process the microstructure and control the re-entrant cauliflower-like micro-ball can be controlled by the process parameters. Droplets of 5 µl of *n*-decane show contact angles of > 155° on the as-prepared superoleophobic surface, and air pockets can be clearly seen underneath, representing a stable Cassie state.

2 Experimental Section

2.1 Materials

Copper sheets with a thickness of 0.8 mm and purity of over 99% were bought online. Anhydrous ethanol was supplied by Jiangtian Chemical Technology Co., Ltd. (Tianjin, China). Analytical-grade sodium hydroxide (NaOH), *n*-decane, ammonium peroxodisulfate [$(NH4)_2S_2O_8$], and hydrochloric acid (HCl) were purchased from Shanghai Aladdin

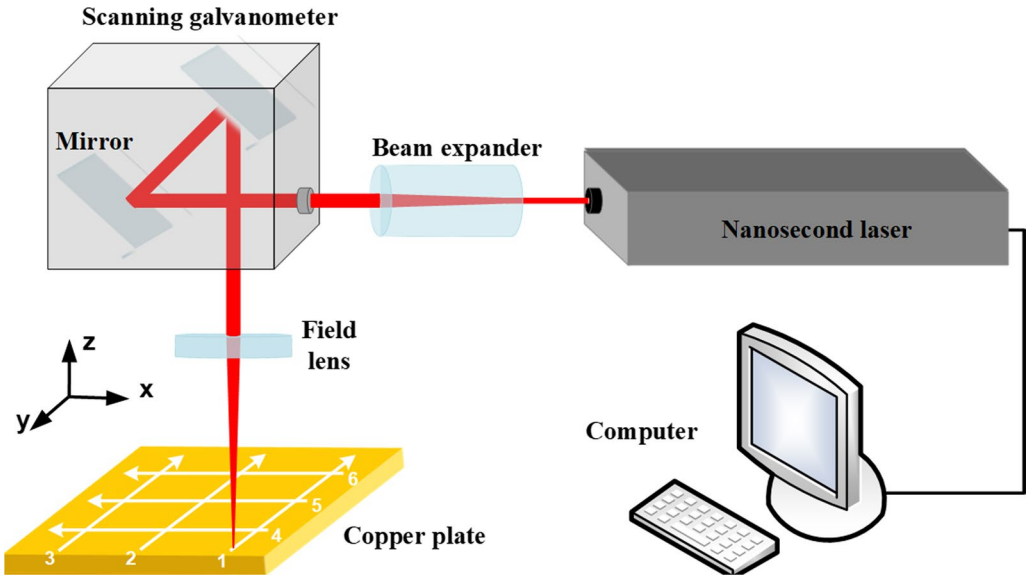

Fig. 1 Schematic of surface ablation on the copper plate surface by a nanosecond laser

Bio-Chem Technology Co., Ltd. A highly fluorinated thiol (purity ≥ 97%) of 1*H*,1*H*,2*H*,2*H*-perfluorodecanethiol (PFDT) was purchased from Alfa Aesar. The distilled water was provided by a UCP-III water purification system. All chemicals (AR level) were used as received without further purification.

2.2 Preparation of Microcone Arrays

A 0.8-mm-thick copper sheet (purity ≥ 99.7%, commercially available) was cut into 10 mm × 10 mm × 0.8 mm samples. After deep washing with ethyl alcohol in an ultrasonic cleaner for 10 min, the copper plate samples were processed by a nanosecond ytterbium fiber laser machine (IPG Photonics, Germany) with 50-ns pulse duration, 1064-nm wavelength, 20-kHz pulse repetition, and 20-W maximum average power. The schematic process of surface texturing is shown in Fig. 1. The laser was focused on the surface of the samples, and it scanned vertically at a constant speed of 100 mm s^{-1}, a repeating time of 30, an average power of 10 W, and scanning intervals in the *x* and *y* directions of 60 μm. After the laser direct writing process, the oxide on the copper surface needs to be removed via immersion in 1 M diluted hydrochloric acid for 1 min.

2.3 Preparation of Re-entrant Structures with Diverse Sizes

The aforementioned as-prepared samples with a microcone array structure were immersed in a 200-ml well-mixed aqueous solution of 2.5 M NaOH and 0.15 M $(NH_4)_2S_2O_8$ on a heating stage. The temperature was set at 30 °C, which was slightly higher than the ambient temperature, to accelerate the reaction rate, as shown in Fig. 2a (step 2). The alkali-assisted oxidation time was set at 30 min and 1 h. If the oxidation time was not mentioned, the default value was 30 min. After the oxidation reaction, the samples were flushed with distilled water and dried in an oven at 110 °C for 10 min.

After the alkali-assisted oxidation, the samples were immersed in a 1 M ethanol solution of PFDT for 10, 30, 50, 70, and 90 min. Then, the samples were flushed with anhydrous ethanol and dried in an oven at 110 °C for 30 min.

2.4 Instruments and Characterization

The surface microtopography of all the samples was observed by a field emission scanning electron microscope (SEM, SUPRA 55 Sapphire, Zeiss, Germany). The contents of the elements were analyzed with an energy-dispersive spectroscope (EDS, Oxford, Germany). Oil droplets were directly dropped onto the surface of the samples in the atmospheric environment to investigate their oil repellency. The contact angles of the 5-μl *n*-decane droplets were measured by an optical contact angle meter (ASTVCM Optima, USA).

3 Results and Discussion

After the laser direct writing process, as shown in Fig. 2a (step 1), the microcone arrays were preliminarily obtained. Then, the samples were ultrasonically washed with 1 M

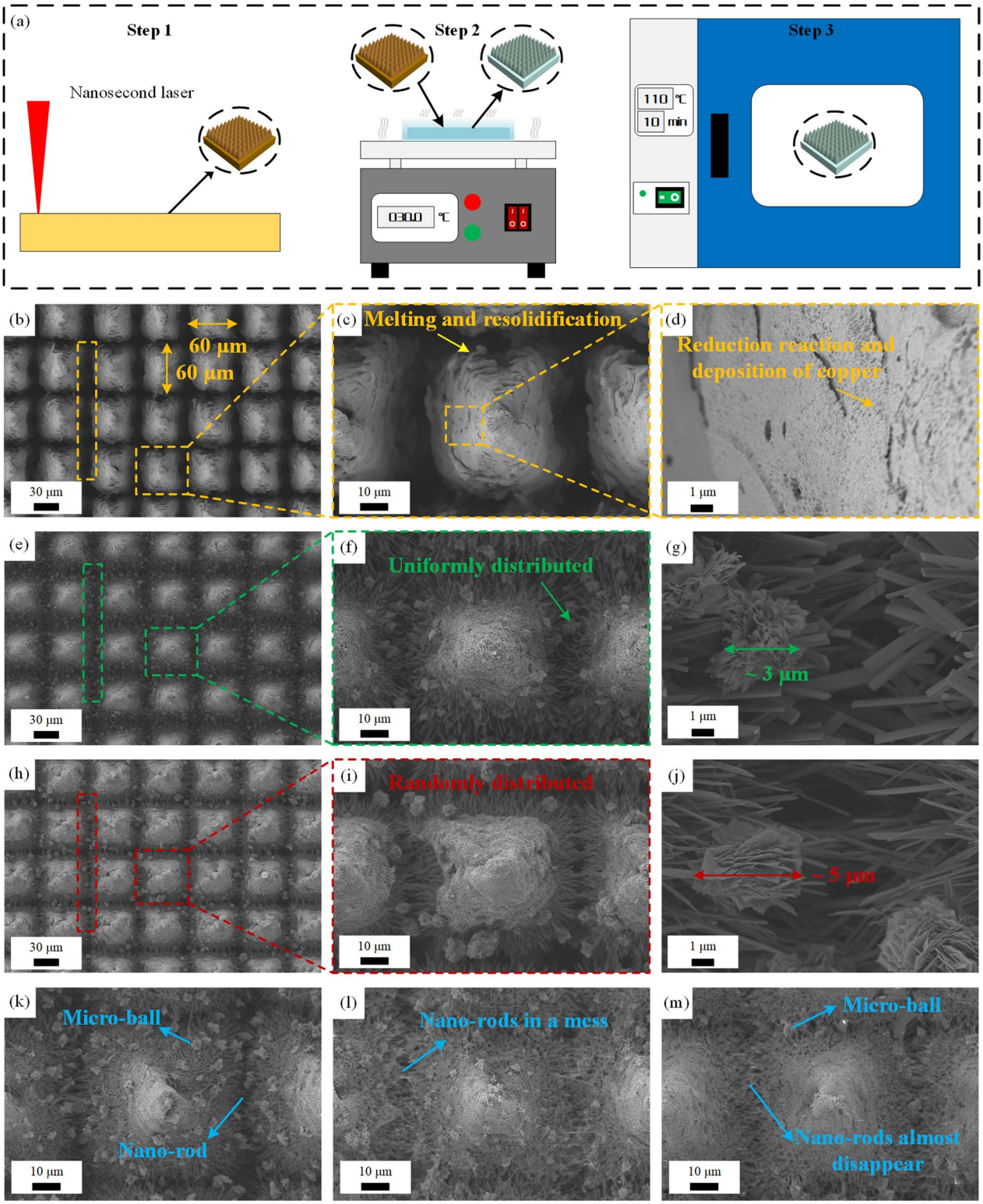

Fig. 2 **a** Steps of the re-entrant structure fabrication process, **b–d** SEM images of laser-ablated microcone arrays in different magnifications, **e–g** SEM images of microcone arrays after 30 min of alkali-assisted oxidation, **h–j** SEM images of microcone arrays after 1 h of alkali-assisted oxidation, **k–m** SEM images of microcone arrays after 30 min of alkali-assisted oxidation followed by 10, 30, 50, 70, and 90 min perfluorothiolate reaction, respectively

diluted hydrochloric acid for 1 min to remove the copper oxide. The chemical reaction goes as follows:

$$CuO + 2HCl \rightarrow CuCl_2 + H_2O$$

$$Cu_2O + 2HCl \rightarrow Cu + CuCl_2 + H_2O$$

The SEM images of the samples after laser processing followed by copper oxide elimination are shown in Fig. 2b–d. We can obviously see the orderly microcone array in Fig. 2b, and the image of a randomly selected microcode is magnified in Fig. 2c. After cleaning using a diluted hydrochloric acid solution, the surface of the microcode seems smooth in spite of the presence of some micro-wave structures caused by the melting and resolidification of copper because of the heat effect of the nanosecond laser. In Fig. 2d, we can further observe nanoparticles, which may be caused by the reduction reaction and deposition of copper when washed by diluted hydrochloric acid or copper resolidification during the laser ablation process. The obtained microcone structure serves as the main body of the functionalized surface to have a huge effect in enlarging the reacting area in the chemical immersion reaction, reducing the contacting area between the liquid and solid surfaces and enhancing the surface robustness [37].

The as-prepared samples with a microcone array structure were immersed in a 200-ml well-mixed aqueous solution of 2.5 M NaOH and 0.15 M $(NH_4)_2S_2O_8$ on a heating stage, as shown in Fig. 2a (step 2). The alkali-assisted oxidation process is presented as follows [38–40]:

$$Cu + 4NaOH + (NH_4)_2S_2O_8 \rightarrow Cu(OH)_2 + 2Na_2SO_4 + 2NH_3 \uparrow + 2H_2O$$

After alkali-assisted oxidation for 30 min, we dried the sample in an oven at 110 °C for 10 min, which was totally different from previous works, as shown in Fig. 2a (step 3). Normally, after the oxidation reaction, the samples would be dried with high-pressure nitrogen at room temperature. In 2019, Pan et al. obtained $Cu(OH)_2$ nanorods on microcones; the samples underwent 20 min of alkali-assisted oxidation and were dried with high-pressure nitrogen [41, 42]. To gain micro-ball structures on the microcones, the chemical oxidation was performed at 90 °C for 50 min. In the present work, after oven-drying at 110 °C, the surface topography was obviously different from those of other works. As shown in Fig. 2e and f, the half bottom of the microcone is full of uniformly distributed nanorods and micro-balls. However, on the top half of the microcone, the nanorods seem to disappear and turn to nano-grass, with a very short length resulting from the high-temperature drying process. Compared with the image in Fig. 2b, the bottom of the trench between two microcones is full of micro/nanostructure in Fig. 2e. By contrast, we continued to take laser-ablated samples to have 1 h of alkali-assisted oxidation and then dried them in an oven at 110 °C for 10 min. As shown in Fig. 2h and i, the micro/nanostructure is distributed on the surface; however, the micro-balls seem bigger but less in number than those in Fig. 2e and f. In Fig. 2g and j, the difference in micro-balls generated by different oxidation time periods can be clearly seen. In Fig. 2g, the randomly selected micro-ball diameter is ~ 3 μm, and the micro-ball constitutes several nano-grasses. In Fig. 2j, the randomly selected micro-ball generated after 1 h of oxidation has a diameter of roughly 5 μm, and this micro-ball constitutes several nanosheets. Furthermore, the nanorods in Fig. 2j are obviously thinner than those in Fig. 2g. Hence, as the oxidation time goes by, the nanorods gradually turn into micro-balls composed of nano-grass and then accumulate into bigger micro-balls constituting nanosheets [42]. The micro-ball acts as a re-entrant structure, and it shows a great importance in fabricating superoleophobic surfaces.

Although the re-entrant micro-ball was generated on the microcone surface, the sample showed superhydrophilic and superoleophilic properties because of the high sample surface energy and its roughness. Here, we propose an approach to fabricate superoleophobic surfaces utilizing PFDT. The samples after alkali-assisted oxidation were immersed in an ethanol solution of PFDT (roughly 1 M) for 10, 30, 50, 70, and 90 min to determine how the fluoridation time influences the superoleophobicity. The perfluorothiolate reaction between $Cu(OH)_2$ and PFDT can be written by referring to the reaction between $Cu(OH)_2$ and alkyl thiols. The equation of the perfluorothiolate reaction is as follows [43]:

$$Cu(OH)_2 + 2CF_3(CF_2)_7(CH_2)_2SH \rightarrow Cu(SC_2H_4C_8F_{17})_2 + 2H_2O$$

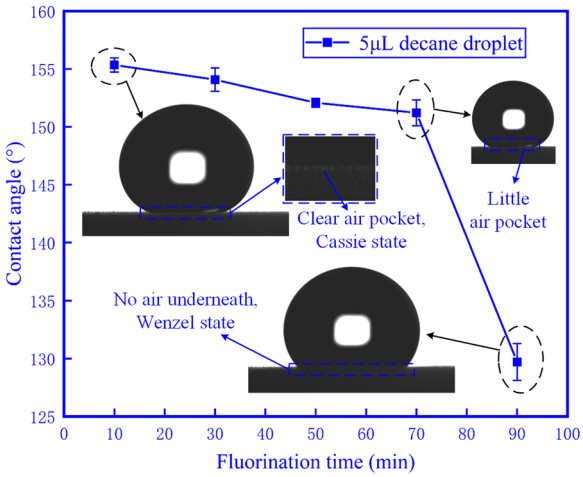

Fig. 3 Contact angle of the prepared sample with different fluoridation times

As shown by the SEM images in Fig. 2k–m, the micro-balls gradually disappear with the increase in the fluoridation time. When the fluoridation time is 10 min, as shown in Fig. 2k, the micro-balls with a diameter of ~ 3 μm are uniformly distributed on the surface of the microcone except at the top of it, and the nanorods do not have obvious changes, as compared with those shown in Fig. 2f. When the fluoridation time increases to 30 min, as shown in Fig. 2l, the number of micro-balls dramatically decreases, and so does the size of the micro-balls. In addition, the nanorods seem in a mess. When the fluoridation time continues to increase to 50 min, as shown in Fig. 2m, little micro-balls can be found on most areas of the microcone surface, only a few microcones exit at the junction of two microcones, and the nanorods barely exist anymore. As time continues to increase, almost all micro-balls disappear.

The oil contact angles of the above-mentioned five samples were measured. As shown in Fig. 3, droplets of 5 μl of *n*-decane were placed on the as-prepared samples. When the fluoridation time is 10 min, the contact angle is ~ 155°, and in the picture, we can clearly see the air pocket between the oil droplet and sample surface, which corresponds to the Cassie state. This phenomenon indicates a stable oil-repellent ability with little liquid–solid contact area. As the fluoridation time increases to 70 min, the oil contact angle decreases slightly, but it is still above 150°. Moreover, the air pocket becomes less obvious because of the reduction of micro-balls. When the fluoridation time increases from 70 to 90 min, the contact angle shows a significant reduction to roughly 130°, and the air pocket completely vanishes. Therefore, the Wenzel state is formed, and the oil droplet cannot leave without any loss. Thus, by controlling the fluoridation time, we can control the number of micro-balls and then the superoleophobicity.

In a previous experiment, we found that PFDT can have a reaction with the product of the alkali-assisted oxidation (mainly $Cu(OH)_2$ in this experiment), and this can definitely affect the wetting ability of the sample surface. Thus, the cooperation of chemical immersion, including the alkali-assisted oxidation reaction time and perfluorothiolate reaction time, was further investigated. From the former experiment, when the oxidation time was set at 30 min, the superoleophobicity of the sample decreased with the increase in the fluoridation time. However, if the fluoridation time was long enough (e.g., 2 h), with the increase in the oxidation time, the superoleophobicity could be enhanced. To make the role of the re-entrant structure in superoleophobic surface fabrication prominent, the influence of microcone spacing was also researched. In Fig. 4, values in the *x* direction represent the microcone spacing, and values in the *y* direction represent the different cooperation of the chemical immersion time. Regardless of the difference in microcone spacing, samples that underwent 30 min of oxidation and 2 h of fluoridation showed the Wenzel state when droplets of 5 μl of *n*-decane were placed on the sample surfaces. However, if the oxidation time increased to 1 h while the fluoridation time remained unchanged, the *n*-decane droplet on the surfaces turned to the Cassie state. Therefore, if the chemical immersion time can have an optimal combination, the as-prepared sample surface can repel an oil droplet, which has low surface tension. When the chemical immersion time combination was set at 1 h of oxidation and 2 h of fluoridation, the contact angle of the *n*-decane droplets on the sample surfaces had little change with the increase in microcone spacing, the Cassie state remained, and the air pocket always existed.

The EDS spectrum was tested to detect the content of five elements, namely C, O, F, S, and Cu, during the fabrication

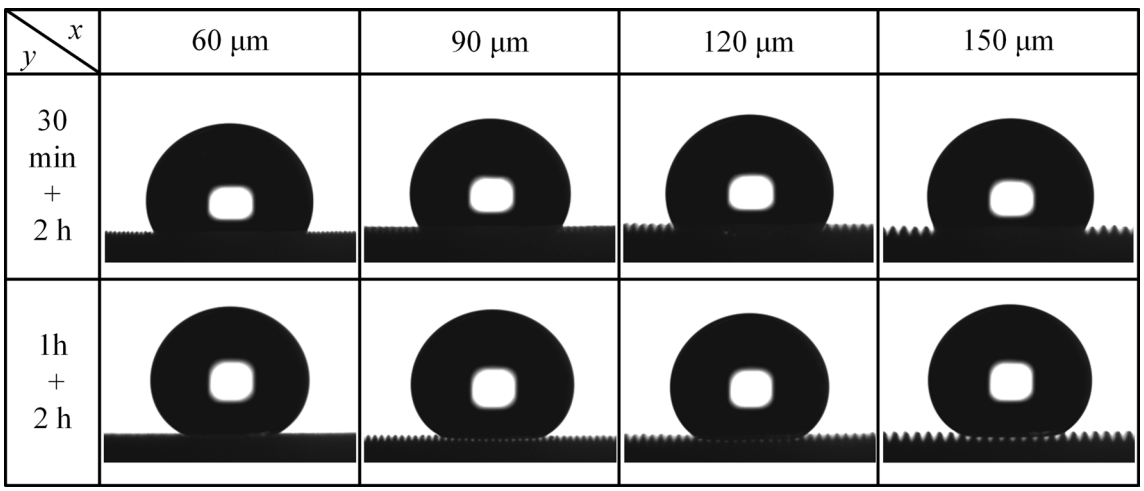

Fig. 4 Contact angle comparison as influenced by microcone spacing (*x* direction) and cooperation of chemical immersion time (*y* direction, oxidation time + fluoridation time)

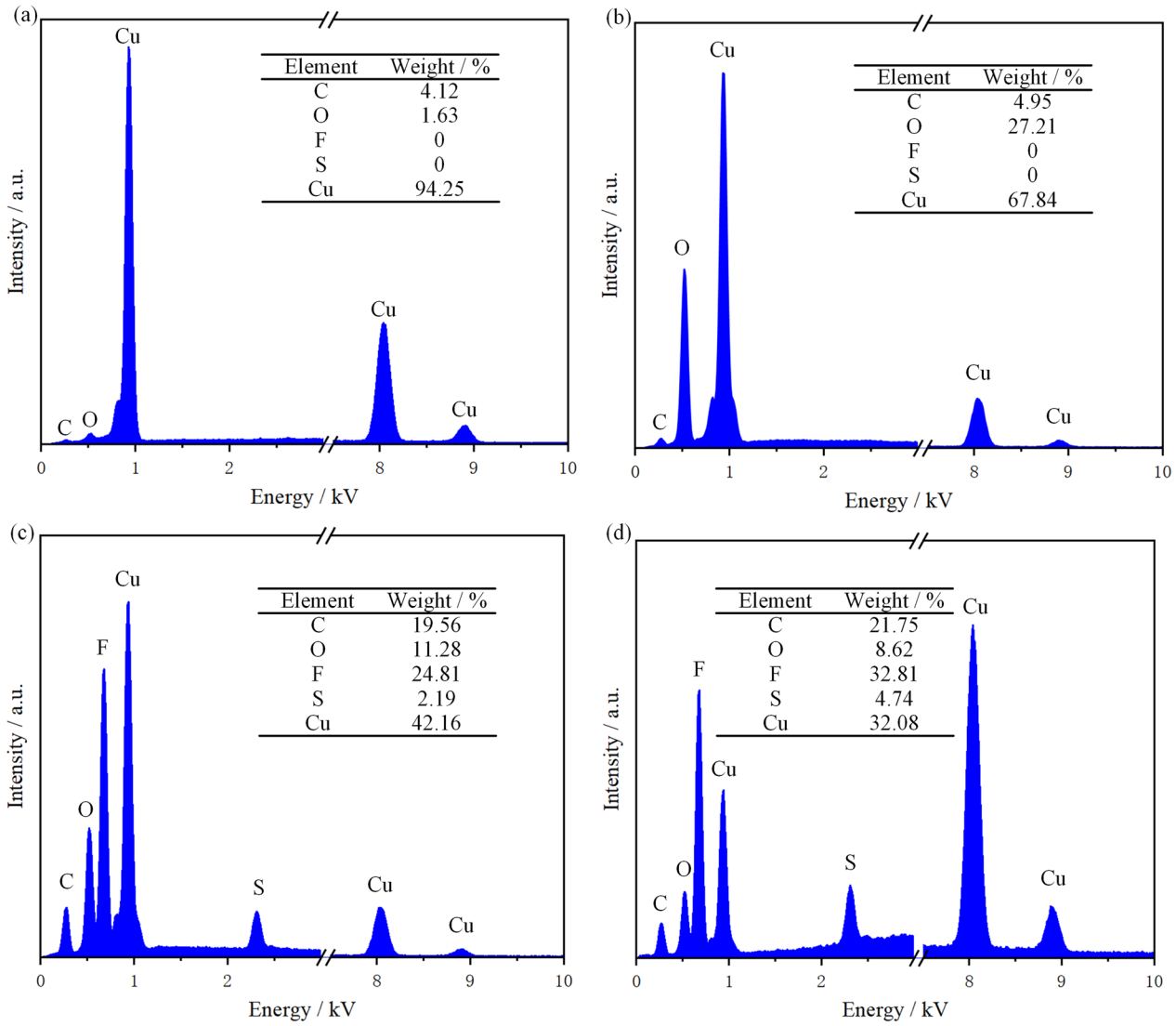

Fig. 5 EDS spectra of **a** the original copper sample with microcone arrays, **b** sample after 30 min of oxidation, **c** sample after 30 min of oxidation followed by 10 min of fluoridation, **d** sample after 30 min of oxidation followed by 90 min of fluoridation

process. Four representative EDS spectra were selected, as shown in Fig. 5. In Fig. 5a, after cleaning with diluted hydrochloric acid, the laser-ablated copper plate had little C and O on its surface. The element of Cu accounted for 94.25% of the weight of the whole surface, and No F and S were also found. After 30 min of alkali-assisted oxidation, the proportion of O dramatically increased from 1.63% to 27.21%, as shown in Fig. 5b, and this mainly resulted from the formation of oxides on the surface. The content of C roughly remained unchanged, and no elements of F and S were detected on the surface. In Fig. 5c, the EDS spectrum obviously changed as compared with the above two spectra. We can also find a large increase of the C element after 10 min of fluoridation, and the F and S elements appeared and increased a lot. The augment of the C, F, and S elements originated from PFDT, which means that the $-CF_3/-CF_2-$ groups were successfully bonded on the sample surface by the perfluorothiolate reaction. In Fig. 5d, when the fluoridation time continued to increase to 90 min, the contents of C, F, and S all showed an increase. On the contrary, the proportion of O and Cu elements decreased. However, due to the limits on the content of oxidation products caused by the limited oxidation time, the increase of the F element was not

as obvious as the first 10-min fluoridation reaction. Hence, the perfluorothiolate reaction can introduce low-surface-energy functional groups to the surface, and proper cooperation of the chemical immersion time has the potential to further decrease the whole surface energy of the surface.

4 Conclusions

In summary, a laser–chemical hybrid method to fabricate superoleophobic surfaces is reported here, and the diameter of re-entrant micro-balls can be controlled by adjusting the parameter of the chemical immersion reaction. Droplets of 5 µl of *n*-decane on the as-prepared superoleophobic surface showed contact angles of $155 \pm 1°$ with clear air pockets underneath, showing a Cassie state contacting mode. The cooperation of the chemical immersion time, including the alkali-assisted oxidation reaction time and perfluorothiolate reaction time, was discussed. A suitable combination of the chemical immersion time contributed to a good oil-repellent surface. Similar microcone arrays with different cone spacing were also discussed here, and the *n*-decane droplet could stay spherical and maintained in the Cassie state even on the surface with microcone spacing at 150 µm, which greatly highlighted the importance of the re-entrant structure in the fabrication of superoleophobic surfaces. We believe that our research results could be helpful in research on oil repellency for oil droplets with extremely low surface energies (Additional files 1, 2, 3, 4, 5).

Supplementary Information The online version contains supplementary material available at https://doi.org/10.1007/s41871-023-00190-w.

Acknowledgements This work was financially supported by National Postdoctoral Program for Innovative Talents (No. BX20190233), National Natural Science Foundation of China (No. 52105477).

Author Contributions JC: Methodology, formal analysis, investigation, writing—original manuscript. LX: Validation, data curation. ZC: Data curation, methodology. FC: Validation, methodology, supervision, writing—review and editing. FW: Validation, supervision. YT: Writing—review and editing. DZ: Writing—review and editing, resources. All authors read and approved the final manuscript.

Availability of Data and Materials All data that support the findings of this study are included in this manuscript and its supplementary information files.

Declarations

Competing interests The authors declare that they have no known competing financial interests or personal relationships that could have appeared to influence the work reported in this paper.

References

1. Chen F, Wang Y, Tian Y, Zhang D, Song J, Crick CR, Carmalt CJ, Parkin IP, Lu Y (2022) Robust and durable liquid-repellent surfaces. Chem Soc Rev 51:8476–8583. https://doi.org/10.1039/D0CS01033B
2. Hensel R, Neinhuis C, Werner C (2016) The springtail cuticle as a blueprint for omniphobic surfaces. Chem Soc Rev 45:323–341. https://doi.org/10.1039/C5CS00438A
3. Cai Z, Chen F, Tian Y, Zhang D, Lian Z, Cao M (2022) Programmable droplet transport on multi-bioinspired slippery surface with tridirectionally anisotropic wettability. Chem Eng J 449:137831. https://doi.org/10.1016/j.cej.2022.137831
4. Xia L, Chen F, Cai Z, Chao J, Tian Y, Zhang D (2022) Magnet-assisted selective oil removal from water in non-open channel and continuous oil spills clean-up. Sep Purif Technol 282:120119. https://doi.org/10.1016/j.seppur.2021.120119
5. Wang L, Yin K, Deng Q, Huang Q, He J, Duan J (2022) Wetting ridge-guided directional water self-transport. Adv Sci 9:2204891. https://doi.org/10.1002/advs.202204891
6. Wang H, Wang Q, Huo L, Liu J, Bai Z (2023) High-efficient laser-based bionic surface structuring for enhanced surface functionalization and self-cleaning effect. Surf Interfaces 37:102691. https://doi.org/10.1016/j.surfin.2023.102691
7. Chen F, Lu Y, Liu X, Song J, He G, Tiwari MK, Carmalt CJ, Parkin IP (2017) Table salt as a template to prepare reusable porous PVDF–MWCNT foam for separation of immiscible oils/organic solvents and corrosive aqueous solutions. Adv Funct Mater 27:1702926. https://doi.org/10.1002/adfm.201702926
8. Wang D, Sun Q, Hokkanen MJ, Zhang C, Lin FY, Liu Q, Zhu SP, Zhou T, Chang Q, He B, Zhou Q, Chen L, Wang Z, Ras RHA, Deng X (2020) Design of robust superhydrophobic surfaces. Nature 582(55):59. https://doi.org/10.1038/s41586-020-2331-8
9. Liu K, Tian Y, Jiang L (2013) Bio-inspired superoleophobic and smart materials: design, fabrication, and application. Prog Mater Sci 58:503–564. https://doi.org/10.1016/j.pmatsci.2012.11.001
10. Jiang T, Guo Z, Liu W (2015) Biomimetic superoleophobic surfaces: focusing on their fabrication and applications. J Mater Chem A 3:1811–1827. https://doi.org/10.1039/C4TA05582A
11. Yong J, Chen F, Yang Q, Huo J, Hou X (2017) Superoleophobic surfaces. Chem Soc Rev 46:4168–4217. https://doi.org/10.1039/C6CS00751A
12. Pan Y, Huang S, Li F, Zhao X, Wang W (2018) Coexistence of superhydrophilicity and superoleophobicity: theory, experiments and applications in oil/water separation. J Mater Chem A 6:15057–15062. https://doi.org/10.1039/c8ta04725a
13. Li F, Kong W, Zhao X, Pan Y (2020) Multifunctional TiO_2-based superoleophobic/superhydrophilic coating for oil−water separation and oil purification. ACS Appl Mater Inter 12:18074–18083. https://doi.org/10.1021/acsami.9b22625

14. Li F, Wang Z, Huang S, Pan Y, Zhao X (2018) Flexible, durable, and unconditioned superoleophobic/superhydrophilic surfaces for controllable transport and oil-water separation. Adv Funct Mater 28:1706867. https://doi.org/10.1002/adfm.201706867
15. Yabu H, Takebayashi M, Tanaka M, Shimomura M (2005) Superhydrophobic and lipophobic properties of self-organized honeycomb and pincushion structures. Langmuir 21:3235–3237. https://doi.org/10.1021/la050013w
16. Feng X, Jiang L (2006) Design and creation of superwetting/antiwetting surfaces. Adv Mater 18:3063–3078. https://doi.org/10.1002/adma.200501961
17. Tsujii K, Yamamoto T, Onda T, Shibuichi S (1997) Super oil-repellent surfaces. Angew Chem Int Edit 36:1011–1012. https://doi.org/10.1002/anie.199710111
18. Shibuichi S, Yamamoto T, Onda T, Tsujii K (1998) Super water- and oil-repellent surfaces resulting from fractal structure. J Colloid Interf Sci 208:287–294. https://doi.org/10.1006/jcis.1998.5813
19. Li H, Wang X, Song Y, Liu Y, Li Q, Jiang L, Zhu D (2001) Super-"amphiphobic" aligned carbon nanotube films. Angew Chem Int Edit 40:1743–1746. https://doi.org/10.1002/1521-3773(20010504)40:9%3c1743::AID-ANIE17430%3e3.0.CO;2-%23
20. Xie Q, Xu J, Feng L, Jiang L, Tang W, Luo X, Han CC (2004) Facile creation of a super-amphiphobic coating surface with bionic microstructure. Adv Mater 16:302–305. https://doi.org/10.1002/adma.200306281
21. Song J, Pan W, Wang K, Chen F, Sun Y (2020) Fabrication of micro-reentrant structures by liquid/gas interface shape-regulated electrochemical deposition. Int J Mach Tool Manu 159:103637. https://doi.org/10.1016/j.ijmachtools.2020.103637
22. Gou X, Guo Z (2019) Surface topographies of biomimetic superamphiphobic materials: design criteria, fabrication and performance. Adv Colloid Interfac Sci 269:87–121. https://doi.org/10.1016/j.cis.2019.04.007
23. Tuteja A, Choi W, Ma M, Mabry JM, Mazzella SA, Rutledge GC, McKinley GH, Cohen RE (2007) Designing superoleophobic surfaces. Science 318:1618–1622. https://doi.org/10.1126/science.1148326
24. Nosonovsky M, Bhushan B (2016) Why re-entrant surface topography is needed for robust oleophobicity. Philos Trans R Soc A: Math Phys Eng Sci 374:20160185. https://doi.org/10.1098/rsta.2016.0185
25. Liu TL, Kim C-JC (2014) Turning a surface superrepellent even to completely wetting liquids. Science 346:1096–1100. https://doi.org/10.1126/science.1254787
26. Liimatainen V, Drotlef DM, Son D, Sitti M (2020) Liquid-superrepellent bioinspired fibrillar adhesives. Adv Mater 32:2000497. https://doi.org/10.1002/adma.202000497
27. Liu H, Wang Y, Huang J, Chen Z, Chen G, Lai Y (2018) Bioinspired surfaces with superamphiphobic properties: concepts, synthesis, and applications. Adv Funct Mater 28:1707415. https://doi.org/10.1002/adfm.201707415
28. Li X, Wang D, Tan Y, Yang J, Deng X (2019) Designing transparent micro/nano re-entrant-coordinated superamphiphobic surfaces with ultralow solid/liquid adhesion. ACS Appl Mater Interfaces 11:29458–29465. https://doi.org/10.1021/acsami.9b08947
29. Ou J, Hu W, Liu S, Xue M, Wang F, Li W (2013) Superoleophobic textured copper surfaces fabricated by chemical etching/oxidation and surface fluorination. ACS Appl Mater Interfaces 5:10035–10041. https://doi.org/10.1021/am402531m
30. Xia L, Chen F, Chao J, Zhang D, Tian Y, Zhang D (2022) Femtosecond laser engineered eggshell membrane for durable oil/water separation under harsh conditions. J Membr Sci 668:121242. https://doi.org/10.1016/j.memsci.2022.121242
31. Yang C, Chao J, Zhang J, Zhang Z, Liu X, Tian Y, Zhang D, Chen F (2020) Functionalized CFRP surface with water-repellence, self-cleaning and anti-icing properties. Colloid Surface A 586:124278. https://doi.org/10.1016/j.colsurfa.2019.124278
32. Shu T, Liu F, Chen S, Liu X, Zhang C, Cheng GJ (2022) Origins of ultrafast pulse laser-induced nano straight lines with potential applications in detecting subsurface defects in silicon carbide wafers. Nanomanuf Metrol 5:167–178. https://doi.org/10.1007/s41871-022-00133-x
33. Wang H, Ma Y, Bai Z, Liu J, Huo L, Wang Q (2022) Evaluation of tribological performance for laser textured surfaces with diverse wettabilities under water/oil lubrication environments. Colloid Surface A 645:128949. https://doi.org/10.1016/j.colsurfa.2022.128949
34. Nakajima A, Omiya M, Yan JW (2022) Generation of micro/nano hybrid surface structures on copper by femtosecond pulsed laser irradiation. Nanomanuf Metrol 5:274–282. https://doi.org/10.1007/s41871-022-00135-9
35. Wang Q, Wang H, Zhu Z, Xiang N, Wang Z, Sun G (2021) Switchable wettability control of titanium via facile nanosecond laser-based surface texturing. Surf Interfaces 24:101122. https://doi.org/10.1016/j.surfin.2021.101122
36. Han J, Cai M, Lin Y, Liu W, Luo X, Zhang H, Zhong M (2018) 3D re-entrant nanograss on microcones for durable superamphiphobic surfaces via laser-chemical hybrid method. Appl Surf Sci 456:726–736. https://doi.org/10.1016/j.apsusc.2018.06.126
37. Wu J, Yin K, Xiao S, Wu Z, Zhu Z, Duan JA, He J (2021) Laser fabrication of bioinspired gradient surfaces for wettability applications. Adv Mater Interfaces 8:2001610. https://doi.org/10.1002/admi.202001610
38. Chen X, Kong L, Dong D, Yang G, Yu L, Chen J, Zhang P (2009) Synthesis and characterization of superhydrophobic functionalized Cu $(OH)_2$ nanotube arrays on copper foil. Appl Surf Sci 255:4015–4019. https://doi.org/10.1016/j.apsusc.2008.10.104
39. Chen X, Kong L, Dong D, Yang G, Yu L, Chen J, Zhang P (2009) Fabrication of functionalized copper compound hierarchical structure with bionic superhydrophobic properties. J Phys Chem C 113:5396–5401. https://doi.org/10.1021/jp809616d
40. Wang L, Tian Z, Jiang G, Luo X, Chen C, Hu X, Zhang H, Zhong M (2022) Spontaneous dewetting transitions of droplets during icing & melting cycle. Nat Commun 13:1–15. https://doi.org/10.1038/s41467-022-28036-x
41. Pan R, Cai M, Liu W, Luo X, Chen C, Zhang H, Zhong M (2019) Extremely high Cassie–Baxter state stability of superhydrophobic surfaces via precisely tunable dual-scale and triple-scale micro–nano structures. J Mater Chem A 7:18050–18062. https://doi.org/10.1039/C9TA04484A
42. Pan R, Cai M, Liu W, Luo X, Chen C, Zhang H, Zhong M (2020) Ultrafast laser hybrid fabrication of hierarchical 3D structures of nanorods on microcones for superhydrophobic surfaces with excellent Cassie state stability and mechanical durability. J Laser Appl 32:022047. https://doi.org/10.2351/7.0000110
43. Yao X, Gao J, Song Y, Jiang L (2011) Superoleophobic surfaces with controllable oil adhesion and their application in oil transportation. Adv Funct Mater 21:4270–4276. https://doi.org/10.1002/adfm.201100775

Jiaqi Chao received the B.Eng. degree in mechanical engineering from Tianjin University of Technology, in 2017, and the M.Sc. degree in mechanical engineering from Tianjin University, in 2021. He is currently working towards the Ph.D. degree in mechanical engineering at the School of Mechanical Engineering, Tianjin University, Tianjin, China. His current research interests include ultrafast laser micro/nano manufacturing, laser-matter interaction, surface science and engineering.

Dr. Faze Chen is an Associate Professor in the School of Mechanical Engineering, Tianjin University. He obtained his PhD in Mechanical Engineering from Dalian University of Technology, China, in 2018. He studied at University College London in 2016 as a visiting researcher for one year. He joined Tianjin University as a postdoctoral fellow and received the grant from National Postdoctoral Program for Innovative Talents in 2019. He has (co-)authored more than 50 high-ranking journals and peer-reviewed conference papers. His research interests focus on functional surfaces with liquid repellence, and laser-based additive/subtractive manufacturing.

Lei Xia received the B.Eng. degree in mechanical engineering from Huanghe S & T University, in 2016, and the M.Sc. degree in mechanical engineering from Tianjin University of Technology, in 2019. He is currently working towards the Ph.D. degree in mechanical engineering at the School of Mechanical Engineering, Tianjin University, Tianjin, China. His current research interests include wettability, interfacial fluid mechanics, droplet impact dynamics.

Zexin Cai received the B.Eng. degree in mechanical engineering from Chongqing University, in 2020, and the M.Sc. degree in mechanical engineering from Tianjin University, in 2023. His current research interests include ultrafast laser processing, bionic functional surface and superslippery surface.

Dr. Fujun Wang received the B.Eng. degree in mechanical engineering from Hebei University of Technology in 2005, and the M.Sc. and Ph.D. degrees in mechanical engineering from Tianjin University, Tianjin, China, in 2007 and 2010, respectively. In 2010, he became an Assistant Professor with the School of Mechanical Engineering, Tianjin University, where he is currently a Distinguished Research Fellow. He was a research scholar in Department of Mechanical Science and Engineering, University of Illinois at Urbana-Champaign, Urbana, USA from 2013 to 2014. His current research interests include micro/nano manipulation and positioning, micro/nano manufacturing, dynamics and control, flexure actuator and robots.

Dr. Yanling Tian received the Ph.D. degree in mechanical engineering from Tianjin University, Tianjin, China, in 2005. He is currently a Professor with Tianjin University. From 2007 to 2009, he was a Research Fellow with Department of Mechanical and Aerospace Engineering, Monash University, Clayton VIC, Australia. He was a Visiting Scholar with the University of Warwick, U.K., in 2006. His research interests include micro/nano manipulation, mechanical dynamics, surface metrology and characterization. Dr. Tian was the recipient of the prestigious Alexander von Humboldt Fellowship for experienced researchers in 2010.

Dr. Dawei Zhang received the B.Eng. degree in mechanical engineering from Shenyang University of Technology, Shenyang, China, in 1984, and the M.Sc. and Ph.D. degrees in mechanical engineering from Tianjin University, Tianjin, China, in 1990 and 1995, respectively. He is currently a Professor with the School of Mechanical Engineering, Tianjin University. He has been a Visiting Scholar at Hongkong University of Science and Technology, Clear Water Bay, Hong Kong; the University of Warwick, Coventry, U.K.; and Tokyo Institute of Technology, Tokyo, Japan. His current research interests include dynamics and machine tools.